Reactive Molecular Dynamics Simulations On Thermal Decomposition of 3-Methyl-2,6-Dinitrophenol

Jiaxiang Zhao
North University of China
Yun Xiao
Hubei Dongfang Chemical Industry Co, Ltd
Jiayuan He
North University of China
Jianlong Wang (wangjianlong@nuc.edu.cn)
North University of China

Research Article

Keywords: 3-Methyl-2,6-dinitrophenol, ReaxFF- force field, thermal decomposition mechanism

Posted Date: November 10th, 2021

DOI: https://doi.org/10.21203/rs.3.rs-1033094/v1

Version of Record: A version of this preprint was published at Journal of Molecular Modeling on January 26th, 2022. See the published version at https://doi.org/10.1007/s00894-022-05036-8.

Abstract

The decomposition mechanism of 3-methyl-2,6-dinitrophenol (MDNP) was simulated by reaction molecular dynamics using ReaxFF force field. The evolution of some main products with time at different heating rates (10, 15 and 20 $K{\cdot}ps^{-1}$) were obtained as well. The simulation outcomes reveal that with the elevation of the heating rate, the shorter the time required for the system to reach equilibrium, and the more products are produced. At three heating rates, the main intermediate products are $C_7H_7O_5N_2$, $C_7H_6O_4N_2$, $C_7H_5O_5N_2$, $C_7H_5O_4N_2$, HON, NO, NO_2 and the primary final products are N_2, CO_2, H_2O, H_2, NH_3, amongst which $C_7H_5O_5N_2$ is the first produced intermediate product and H_2O is the first produced final product with the biggest abundance. The intermediate products first increase and then decrease to zero. Moreover, the primary chemistry reactions in the MDNP pyrolysis are acquired by ReaxFF MD simulations.

1 Introduction

2,2',4,4',6,6'-Hexanitrostiblbenzil (HNBB) is an important intermediate in the preparation of heat-resistant explosive 2,2',4,4',6,6'-hexanitrostiblbene (HNS) [1]. The yield of HNBB is high with TNT as raw material and NaClO as oxidant. 3-Methyl-2,6-dinitrophenol (MDNP) is a by-product separated from the synthesis of HNBB. MDNP is a potential explosive with a density of 1.605 $g{\cdot}cm^{-1}$, oxygen balance of – 88.9% and Nitrogen content of 14.14%. For that reason, to guarantee the safeness of MDNP during usage, research on the thermolysis features and causal links of MDNP is urgently needed.

On the battle field, ammunitions can easily suffer from unforeseen exterior stimulating factors, which might trigger catastrophes during the transport, stockpile and usage of blasting materials. Heat stimuli act as one of the most commonly seen exterior stimulating factors, which might cause the thermolysis of blasting materials and further trigger explosion. As per the thermolysis causal link, the thermal risks of MDNP could be decreased during usage. For that reason, to guarantee the safeness of MDNP during usage, research on thermolysis features and causal links of MDNP is urgently needed. Experiment data are often limited to the information acquired from TGA or TGA/MS, which could merely offer dynamic rate constants of the general mass loss and yield of the eventual gas products,and information on intermediates is not available.

ReaxFF force field is a brilliant technology to explore the thermolysis features and causal links of materials [2], which could well compensate for the experimental flaws. Recently, the ReaxFF force field has been one of the primary technologies to study the thermolysis process of energy materials via reactive force fields [3–8]. Those excellent instances offer vital assistance in the computation of other energy materials [9–13].

In this study, ReaxFF force field is utilized to study the primary middle products, eventual products and chemistry reaction processes at 10 $K{\cdot}ps^{-1}$, 15 $K{\cdot}ps^{-1}$ and 20 $K{\cdot}ps^{-1}$, respectively. The primary middle

products, eventual products and chemistry reaction processes are acquired. On the foundation of the emulated outcomes, the thermolysis causal link of MDNP is acquired.

2. Computational Methods And Simulation Details

2.1 Simulation methodologies

ReaxFF MD emulations are employed to explore the thermolysis of MDNP via ReaxFF-lg force field. ReaxFF, put forward by van Duin [14], offers an almost ab initio level of depiction of the reaction potential surface for multiparticle systems[15]. In the process of ReaxFF MD emulations, the charge and bond orders are computed posterior to each step, which identifies the forming and breaking of covalent linkages. In the process of ReaxFF emulations, the entire atoms were considered individual interactive centers, and the transient dot electric charge on every atom was identified by the static electric field owing to the entire charges around[15]. Chaban et al. [15–18] elucidated the methods of ReaxFF MD in a detailed way, and such a method was successfully used in the past to tackle numerous intricate challenges. For that reason, ReaxFF MD is leveraged to depict the forces on the atoms within the C/H/O/N system herein.

2.2 Temperature-dependent decomposition simulations

In the present research, the LAMMPS was utilized to implement the ReaxFF MD emulations of MDNP (Fig. 1) at 10 K·ps^{-1}, 15 K·ps^{-1} and 20 K·ps^{-1}, respectively. The diffraction data of MDNP are from experimental measurements, which pertains to the monoclinal system with the spacial group of $P2_1/n$, and the crystal parameters of a = 9.59 Å, b = 17.3 Å, c = 9.90 Å, and β = 94.90°. Figure. 2 demonstrates the unit cell (a) and super cell (b) of MDNP. The MDNP super cell was initially completed 10 ps MD emulation with NVT (const. of particulates, volumes, and temperatures) ensemble at 298 K, and afterwards another 10 ps MD emulation was finished with NPT (const. of particulates, pressures, and temperatures) ensemble at 298 K and 0 Pa to remove the inner stress and to acquire the original structure. The relaxed MDNP super cell was afterwards completed 270 ps, 180 ps and 135 ps MD emulations at 10 K·ps^{-1}, 15 K·ps^{-1} and 20 K·ps^{-1}, separately, via NVT ensemble with Berendsen thermostatic device with ReaxFF-lg reaction force field. The intermediate products, eventual products and primary chemistry reaction processes are obtained to explore the thermolysis path of MDNP. In the process of ReaxFF MD emulations, the charge and bond orders are computed posterior to each step, for that reason, a comparatively small integral time ought to be utilized to efficiently cover the phase space enabling the smooth occurrence of collision and reactions. During such emulation, the timestep of every ReaxFF MD emulation was 0.1 fs, and the kinetic path involving atom locations and speeds was documented every 200 fs. Those acquired data were utilized to study the molecule species to offer knowledge pertaining to chemistry reaction processes.

3 Results And Discussion

3.1 Evolution of potential energy (PE) and total number of MDNP

The PE development of MDNP could be applied for judging if the chemistry reactions reach balance, and the sum of MDNP could be applied for assessing the thermolysis level of MDNP. For that reason, the PE of MDNP is subjected to analysis posterior to emulations. PE development of MDNP varies with time at different heating rates are shown in Figure. 3.

Figure. 3 shows the development of total PE with time at different heating rates. MDNP gradually absorbs heat to reach primary decomposition energy at different heating rates. With increasing temperature, the decomposing of MDNP generates a series of middle and eventual products and releases a large amount of heat, so the potential energy decreases significantly. Moreover, if the temperature is elevated, the maximal results of PE and the PE reduction rate will be higher. With the increase of temperature, the greater the stability value of PE, the shorter the time for PE to stabilize. The curves of MDNP show that at 10 $K{\cdot}ps^{-1}$, 15 $K{\cdot}ps^{-1}$ and 20 $K{\cdot}ps^{-1}$, MDNP molecules are converted into intermediate products via decomposition in 178.02 ps, 110.60 ps and 100.00 ps, separately, revealing that faster heating rates trigger more rapid thermolysis of MDNP. The time evolution of consumption of MDNP at various temperatures is displayed in Fig. 4.

3.2 Evolution of intermediate products

In the process of MDNP thermolysis, substantial middle and eventual products were produced. The generative time and the quantity of intermediate and eventual products are pivotal for the investigation of the decomposing process of MDNP. The generative times of the primary intermediate generated by MDNP decomposition are shown in Table. 1-3. Development of the primary intermediate product quantity ($C_7H_7O_5N_2$, $C_7H_6O_4N_2$, $C_7H_5O_5N_2$, $C_7H_5O_4N_2$, HON, NO, NO_2) generated by MDNP decomposition at 10 $K{\cdot}ps^{-1}$, 15 $K{\cdot}ps^{-1}$ and 20 $K{\cdot}ps^{-1}$ are displayed in Figure. 5.

Table 1
Main intermediate products generated by MDNP decomposition at 10 $K{\cdot}ps^{-1}$

Products	Time/ps	Products	Time/ps
MDNP	0	$C_7H_5O_4N_2$	121.52
$C_7H_7O_5N_2$	51.02	HON	152.38
$C_7H_6O_4N_2$	124.74	NO	143.18
$C_7H_5O_5N_2$	51.02	NO_2	121.36

Table 2
Main intermediate products generated by MDNP decomposition at 15 $K \cdot ps^{-1}$

Products	Time/ps	Products	Time/ps
MDNP	0	$C_7H_5O_4N_2$	82.58
$C_7H_7O_5N_2$	40.18	HON	96.46
$C_7H_6O_4N_2$	85.18	NO	92.80
$C_7H_5O_5N_2$	40.2	NO_2	83.46

Table 3
Main intermediate products generated by MDNP decomposition at 20 $K \cdot ps^{-1}$

Products	Time/ps	Products	Time/ps
MDNP	0	$C_7H_5O_4N_2$	60.76
$C_7H_7O_5N_2$	16.54	HON	93.60
$C_7H_6O_4N_2$	60.82	NO	79.02
$C_7H_5O_5N_2$	16.54	NO_2	62.56

We could deduce from Figure. 5 that the quantity of the middle products $C_7H_7O_5N_2$, $C_7H_6O_4N_2$, $C_7H_5O_5N_2$, $C_7H_5O_4N_2$, HON, NO and NO_2 molecules initially raised and afterwards progressively dropped to 0 with the development of the reaction, where high-frequency reactions primarily happened between those middle product molecules till the forming of eventual steady products. The chronology order of the middle product occurrence was $C_7H_5O_5N_2$, $C_7H_7O_5N_2$, $C_7H_5O_4N_2$, $C_7H_6O_4N_2$, NO_2, NO, HON. The order of the maximum number of intermediates is $C_7H_5O_4N_2$, $C_7H_5O_5N_2$, NO_2, HON, NO, $C_7H_7O_5N_2$, $C_7H_6O_4N_2$ at 10 $K \cdot ps^{-1}$. The order of the maximum number of intermediates is $C_7H_5O_5N_2$, NO_2, $C_7H_5O_4N_2$, HON, NO, $C_7H_6O_4N_2$, $C_7H_7O_5N_2$ at 15 $K \cdot ps^{-1}$. The order of the maximum number of intermediates is $C_7H_5O_4N_2$, $C_7H_5O_5N_2$, HON, NO_2, NO, $C_7H_6O_4N_2$, $C_7H_7O_5N_2$ at 20 $K \cdot ps^{-1}$. The order of the number of the maximum intermediates of intermediates under different heating rates is different, in that the reaction time is different at each heating rate, the maximum number of intermediates is different.

$C_7H_7O_5N_2$, $C_7H_6O_4N_2$, $C_7H_5O_5N_2$ and $C_7H_5O_4N_2$ were the primary middle products in the initial thermolysis process of MDNP. With the development of thermolysis, HON, NO and NO_2 turned into the primary middle products. The entire middle products nearly vanished posterior to 2700 K. The quantity of N_2, CO_2, H_2O, H_2 and NH_3 was elevated with the development of the decomposition, revealing that the production of N_2, CO_2, H_2O, H_2 and NH_3 molecules were ongoing in the entire decomposing process.

3.3 Evolution of final products

The entire eventual products were small molecule products like N_2, CO_2, H_2O, H_2, NH_3, etc. The generation times of the main eventual products produced by MDNP thermolysis are shown in Table. 4-6. The development of the quantity of the primary eventual products (N_2, CO_2, H_2O, H_2, NH_3) produced by MDNP thermolysis are displayed in Fig. 6. We could deduce from the emulation outcomes that the chronology order of the final product occurrence was H_2O, H_2, CO_2, N_2, NH_3 at 10 K·ps^{-1}. We could deduce from the emulation outcomes that the chronology order of the final product occurrence was H_2O, H_2, N_2, NH_3, CO_2 at 15 K·ps^{-1} and 20 K·ps^{-1}. The order of the maximum number of eventual products was H_2O, N_2, H_2, CO_2, NH_3 at 10 K·ps^{-1} and 15 K·ps^{-1}. The order of the maximum number of final products is H_2O, N_2, NH_3, H_2, CO_2 at 10 K·ps^{-1} and 15 K·ps^{-1}.

Table 4
Main eventual products produced by MDNP thermolysis at 10 K·ps^{-1}

Products	Time/ps	Products	Time/ps
MDNP	0	H_2	129.66
H_2O	99.70	CO_2	173.50
N_2	183.00	NH_3	207.48

Table 5
Main eventual products produced by MDNP thermolysis at 15 K·ps^{-1}

Products	Time/ps	Products	Time/ps
MDNP	0	H_2	123.42
H_2O	76.70	CO_2	139.66
N_2	137.76	NH_3	138.80

Table 6 Main eventual products produced by MDNP thermolysis at 20 K·ps^{-1}

Products	Time/ps	Products	Time/ps
MDNP	0	H_2	93.96
H_2O	61.22	CO_2	117.26
N_2	106.68	NH_3	116.50

The entire middle products nearly vanished posterior to 135 ps emulations at 20 K·ps^{-1}. The quantity of N_2, CO_2, H_2O, H_2 and NH_3 was elevated with the development of the decomposition, revealing that the production of N_2, CO_2, H_2O, H_2 and NH_3 molecules are undergoing the entire decomposing process.

During the first phase of MDNP thermolysis, there wasn't any production of H_2 and CO_2, which revealed that the decomposing of MDNP didn't generate H_2 and CO_2 straightly, and H_2O and CO_2 were primarily generated by the reactive process between middle products. H_2O occurred at 61.22 ps at 20 $K{\cdot}ps^{-1}$, revealing that some H_2O were possibly produced by MDNP straightly. We could come to the conclusion from Figure. 6 that with the rise of temperature, the quantity of N_2, CO_2, H_2O, H_2, NH_3 was elevated, unveiling that high-temperature facilitated the production of gas products.

For intermediate products, the main decomposition paths of $C_7H_7O_5N_2$ are (1) $C_7H_6O_5N_2 + HON \rightarrow C_7H_7O_6N_3$, (2) $C_7H_7O_6N_3 \rightarrow C_7H_7O_5N_2 + ON$. The main decomposition paths of $C_7H_6O_4N_2$ are (1) $C_7H_6O_5N_2 \rightarrow C_7H_5O_4N_2 + HO$, (2) $C_7H_5O_4N_2 + HON \rightarrow C_7H_6O_5N_3$, (3) $C_7H_6O_5N_3 \rightarrow ON + C_7H_6O_4N_2$. The main decomposition paths of $C_7H_5O_5N_2$ are (1) $C_7H_6O_5N_2 \rightarrow C_7H_5O_4N_2 + HO$, (2) $C_7H_5O_4N_2 + O_2N \rightarrow C_7H_5O_6N_3$, (3) $C_7H_5O_6N_3 \rightarrow C_7H_5O_5N_2 + ON$. The main decomposition path of $C_7H_5O_4N_2$ is $C_7H_6O_5N_2 \rightarrow C_7H_5O_4N_2 + HO$. The main decomposition paths of HON are as follows: (1) $H_2O_2N \rightarrow HON + HO$, (2) $H_3O_2N \rightarrow H_2O + HON$, (3) $C_7H_5O_4N_2 \rightarrow C_7H_4O_3N + HON$. The main decomposition paths of NO are as follows: (1) $H_2O_2N \rightarrow H_2O + ON$,(2) $HO_2N \rightarrow ON + HO$(3) $C_7H_5O_5N_3 \rightarrow C_7H_5O_4N_2 + ON$. The main decomposition paths of NO_2 are (1) $C_7H_5O_5N_2 \rightarrow C_7H_5O_3N + O_2N$(2) $C_7H_5O_6N_3 \rightarrow O_2N + C_7H_5O_4N_2$(3) $H_2O_3N \rightarrow H_2O + O_2N$.

For final products, the main decomposition paths of H_2O are (1) $H_2O_2N \rightarrow H_2O + ON$, (2) $H_3O_2 \rightarrow H_2O + HO$, (3) $H_2ON_2 \rightarrow H_2O + N_2$. The main decomposition paths of N_2 are (1) $H_2ON_2 \rightarrow H_2O + N_2$, (2) $HON_2 \rightarrow N_2 + HO$, (3) $CO_2N_2 \rightarrow N_2 + CO_2$. The main decomposition paths of H_2 are (1) $H_3O \rightarrow H_2 + HO$, (2) $H_2ON \rightarrow H_2 + ON$. The main decomposition paths of CO_2 are as follows: (1) $CO_2N_2 \rightarrow N_2 + CO_2$, (2) $CO_3N \rightarrow CO_2 + ON$, (3) $CH_3O_2N \rightarrow H_3N + CO_2$. The main decomposition paths of NH_3 are as follows: (1) $H_4ON \rightarrow H_3N + HO$, (2) $H_5ON \rightarrow H_2O + H_3N$, (3) $H_3ON_2 \rightarrow H_3N + ON$.

4 Conclusion

ReaxFF MD emulations were employed to explore the thermolysis process of MDNP. The primary middle products were $C_7H_7O_5N_2$, $C_7H_6O_4N_2$, $C_7H_5O_5N_2$, $C_7H_5O_4N_2$, HON, NO, NO_2 and the primary eventual products were N_2, CO_2, H_2O, H_2, NH_3. The chronology order of the occurrence of the middle products was $C_7H_7O_5N_2$, $C_7H_5O_5N_2$, $C_7H_5O_4N_2$, $C_7H_6O_4N_2$, NO_2, NO, HON. The chronology order of the occurrence of the final products was H_2O, H_2, N_2, NH_3, CO_2. Those outcomes verified that ReaxFF could offer deep inspirations as to the intricate reactive processes in MDNP thermal decomposition, and it serves as an attractive approach to explaining the chemistry reaction processes in the thermal decomposition of MDNP with more details.

Declarations

Funding: No funding was received.

Conflicts of interest/Competing interests: The authors declare that they have no known competing financial interests or personal relationships that could have appeared to influence the work reported in this paper.

Availability of data and material: The datasets generated during and/or analysed during the current study are available from the corresponding author on reasonable request.

Code availability: In this study, the large-scale atomic/molecular massively parallel simulator (LAMMPS) was adopted.

Authors' contributions: Jiaxiang Zhao performed the data analyses and wrote the manuscript; Yun Xiao contributed to the conception of the study; Jiayuan He performed the experiment; Jianlong Wang helped perform the analysis with constructive discussions.

References

1. Williams DL (2009) A determination of the hansen solubility parameters of hexanitrostiblbene. Propell. Explos. Pyrot. 5:8–11
2. Cheng XM, Wang QD, Li JQ, Wang JB, Li XY (2012) ReaxFF molecular dynamics simulations of oxidation of toluene at high temperatures. J. Phys. Chem. A. 116:9811–8.
3. Yanilkin AV, Sergeev OV (2014) Molecular dynamics simulation of combustion front propagation in a PETN single crystal. Combust Explo and Shock^{+}. 50:323–332.
4. Zhou T, Huang F (2011) Effects of defects on thermal decomposition of HMX via ReaxFF molecular dynamics simulations. J. Phys. Chem. B. 115:278–287.
5. Rom N, Zybin SV, Van Duin ACT, Goddard WA, Zeiri Y, Katz. G, Kosloff R (2011) Density-dependent liquid nitromethane decomposition: molecular dynamics simulations based on ReaxFF. J. Phys. Chem. A. 115:10181–10202.
6. Müller J, Hartke B (2016) ReaxFF reactive force field for disulfide mechanochemistry, fitted to multireference ab initio data. J. Chem. Theory Comput. 12:3913–3925.
7. Senftle TP, Hong S, Islam MM, Kylasa SB, Zheng Y, Shin YK, Junkermeier C, Engel-Herbert R, Janik MJ, Aktulga HM, Verstraelen T, Grama TA, Van Duin ACT (2016) The ReaxFF reactive force-field: development, applications and future directions. npj Comput. Mater. 2:15011.
8. Liu L, Liu Y, Zybin S V, Sun H, Goddard WA (2011) ReaxFF-lg: correction of the ReaxFF reactive force field for London dispersion, with applications to the equations of state for energetic materials. J. Phys. Chem. A. 115:11016–11022.
9. Nomura KI, Kalia RK, Nakano A, Vashishta P, Van Duin AC (2007) Dynamic transition in the structure of an energetic crystal during chemical reactions at shock front prior to detonation. Phys. Rev. Lett. 99:148303.
10. Zhang LZ, Zybin SV, Van Duin ACT, Goddard WA (2010) Modeling high rate impact sensitivity of perfect RDX and HMX crystals by ReaxFF reactive dynamics. J. Energ. Mater. 28:92–127.

11. Wen YS, Xue XG, Zhou XQ, Guo F, Long XP, Zhou Y, Li HZ, Zhang CY (2013) Twin Induced sensitivity enhancement of HMX versus shock: a molecular reactive force field simulation. J. Phys. Chem. C. 117:24368–24374.
12. Wood MA, Van Duin ACT, Strachan A (2014) Coupled thermal and electromagnetic induced decomposition in the molecular explosive α-HMX; a reactive molecular dynamics study. J. Phys. Chem. A. 118:885–895.
13. Lan GC, Li J, Zhang GY, Ruan J, Lu ZY, Jin SH, Cao DL, Wang JL (2021) Thermal decomposition mechanism study of 3-nitro-1,2,4-triazol-5-one (NTO): Combined TG-FTIR-MS techniques and ReaxFF reactive molecular dynamics simulations. FUEL. 295:120655.
14. Van Duin ACT, Dasgupta S, Lorant F, Goddard WA (2001) ReaxFF: a reactive force field for hydrocarbons. J. Phys. Chem. A. 105:9396–409.
15. Chaban VV, Pal S, Prezhdo OV (2016) Laser-induced explosion of nitrated carbon nanotubes: nonadiabatic and reactive molecular dynamics simulations. J. Am. Chem. Soc. 138:15927–34.
16. Chaban VV, Prezhdo OV (2016) Haber process made efficient by hydroxylated graphene: Ab initio thermochemistry and reactive molecular dynamics. J. Phys. Chem. Lett. 7:2622–6.
17. Chaban VV, Fileti EE, Prezhdo OV (2015) Buckybomb: reactive molecular dynamics simulation. J. Phys. Chem. Lett. 6:913–7.
18. Chaban VV, Prezhdo OV (2016) Energy storage in cubane derivatives and their real-time decomposition: computational molecular dynamics and thermodynamics. ACS. Energy. Lett. 1:189–94.

Figures

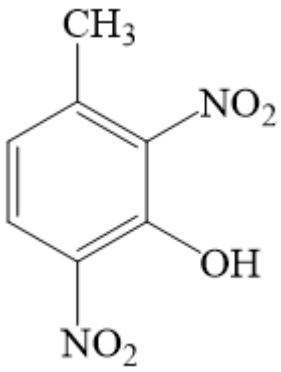

Figure 1

Molecular structures for MDNP

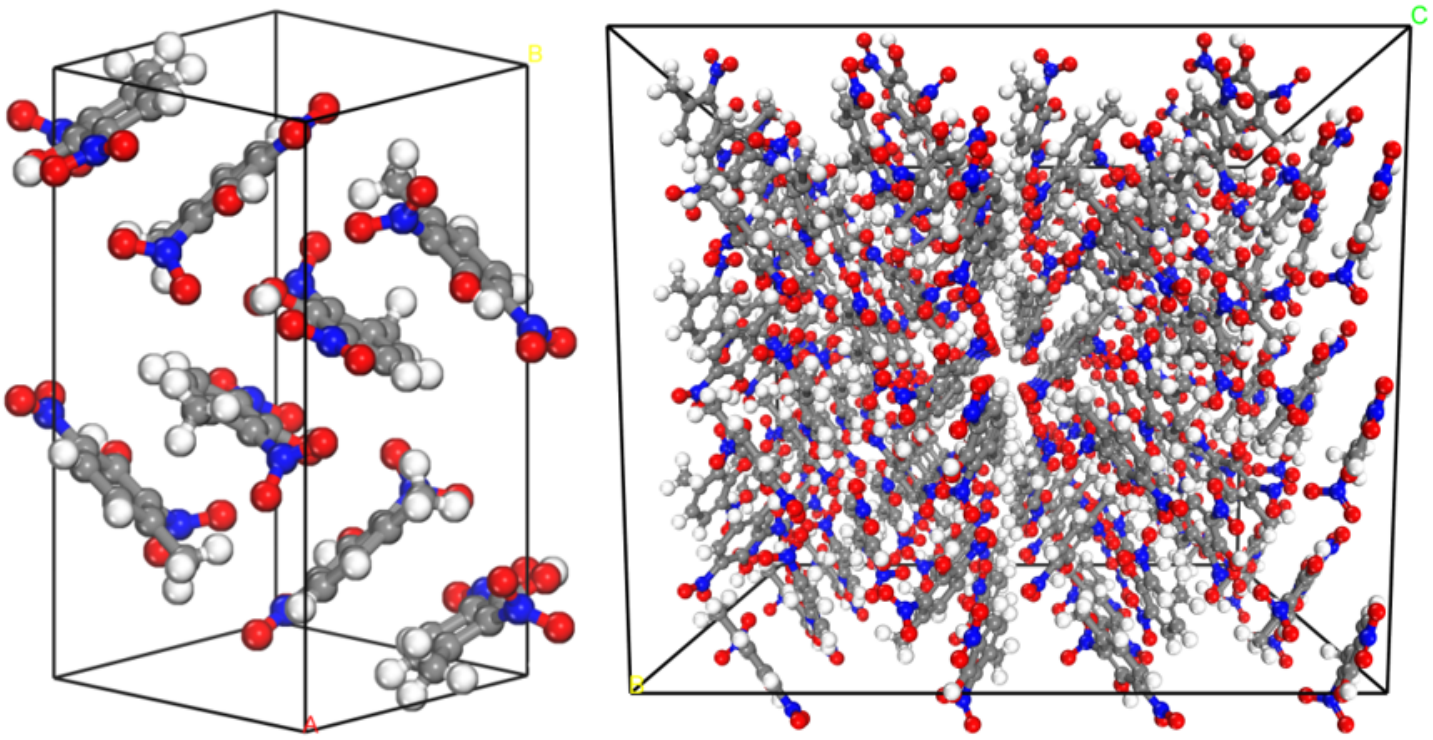

Figure 2

The unit cell and supercell structures of MDNP

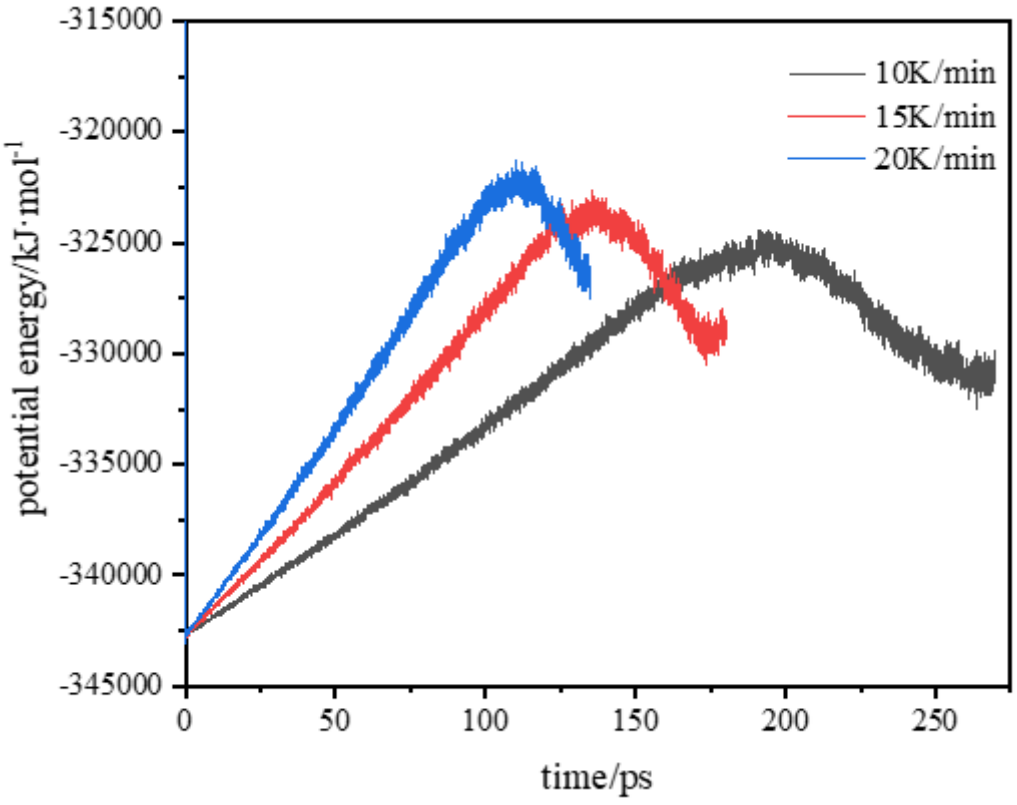

Figure 3

Time evolution of PE at different temperatures

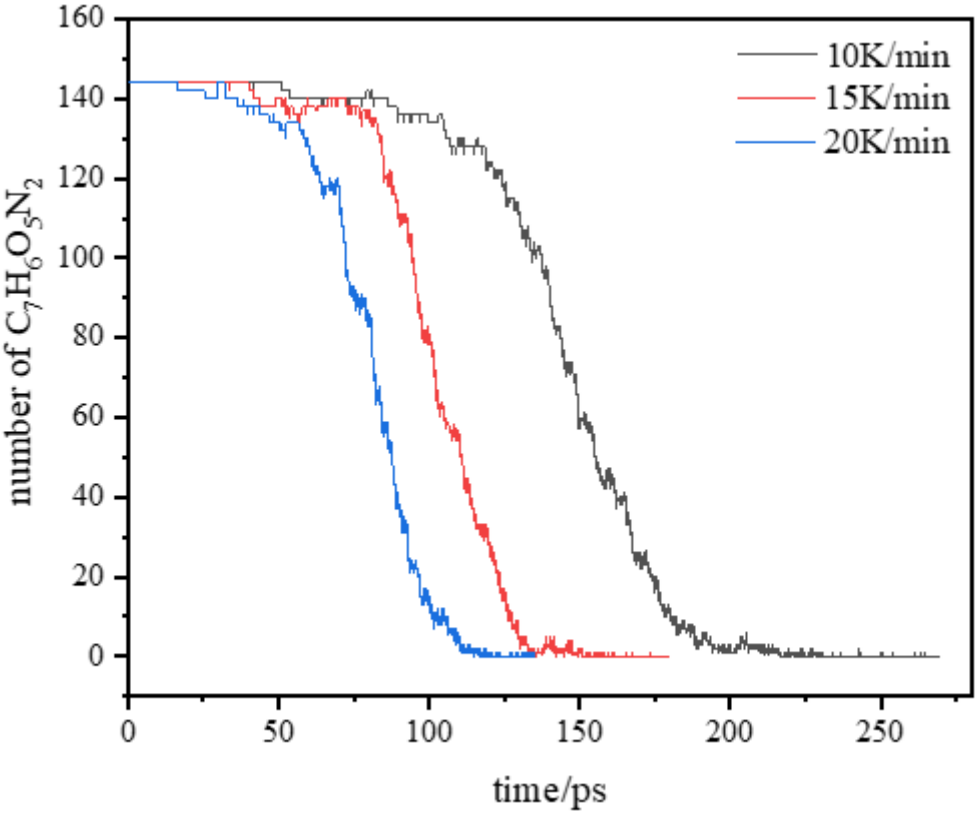

Figure 4

Time evolution of consumption of MDNP at various temperatures

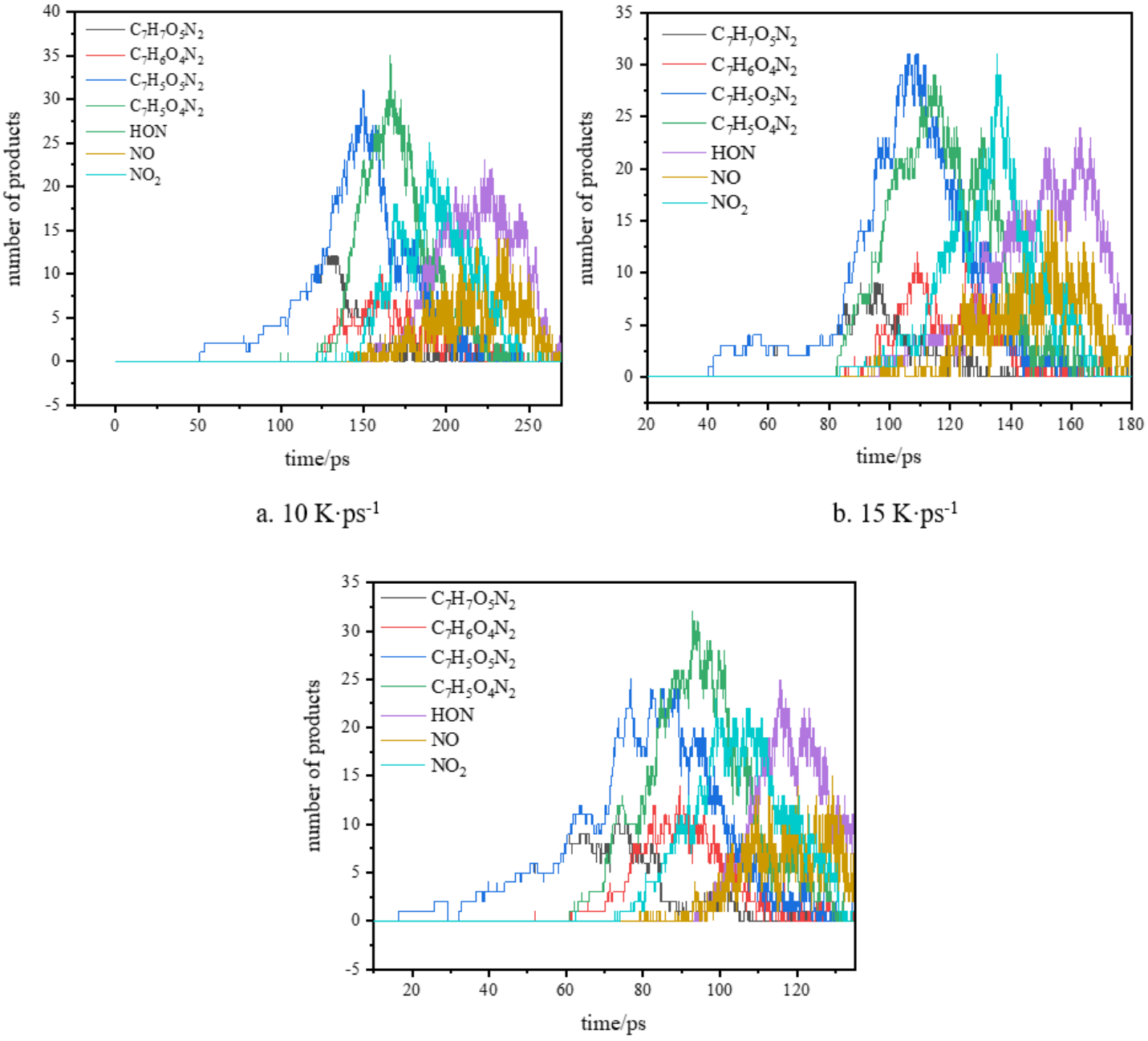

a. 10 K·ps^{-1}

b. 15 K·ps^{-1}

c. 20 K·ps^{-1}

Figure 5

Comparative distribution curves of main intermediate product at various temperatures

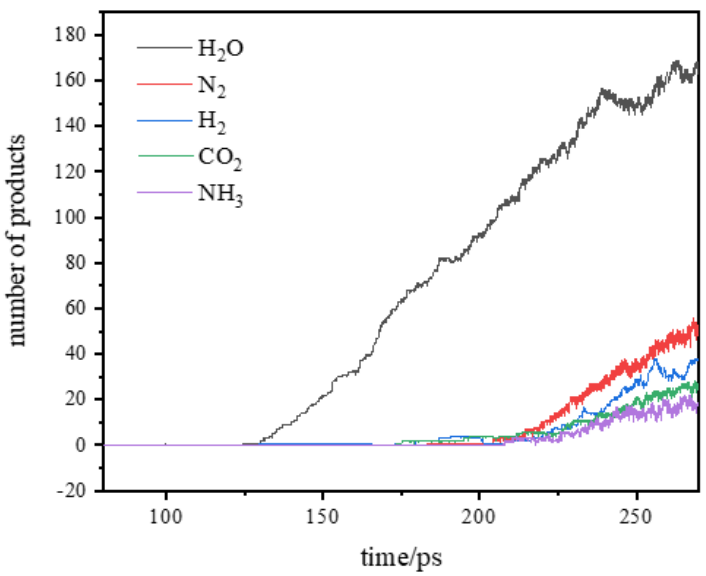

a. 10 K·ps^{-1}

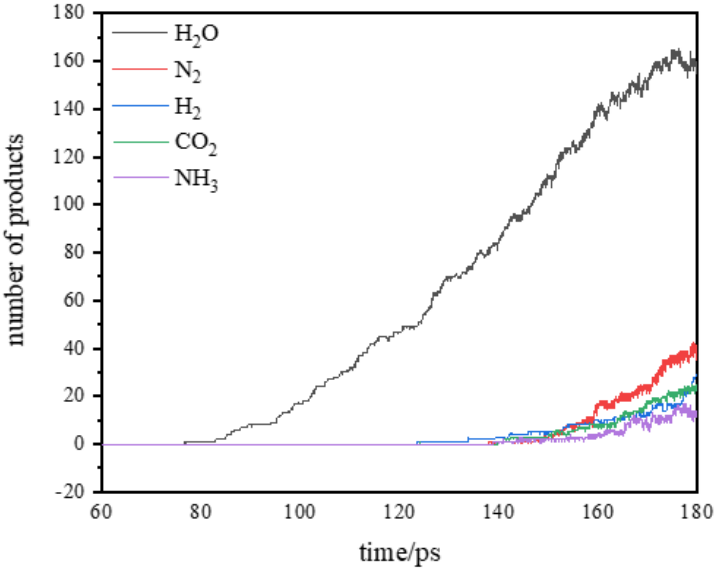

b. 15 K·ps^{-1}

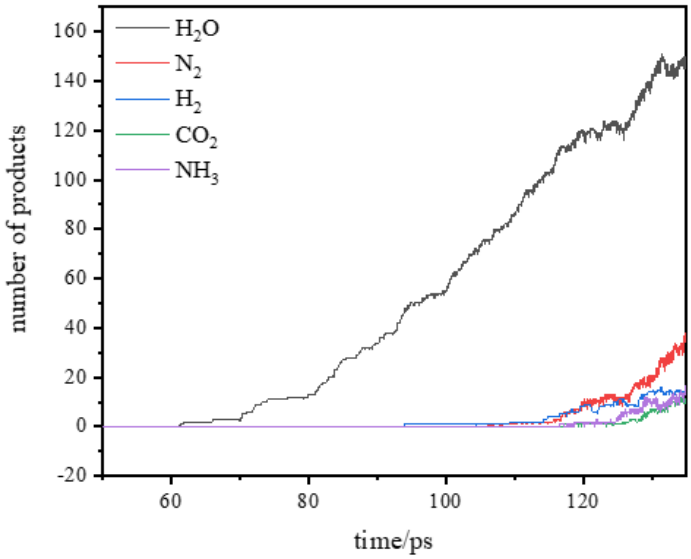

c. 20 K·ps^{-1}

Figure 6

Comparative distribution curves of main final product at various temperatures